Liquid Spreading under Nanoscale Confinement

Antonio Checco*

Condensed Matter Physics and Materials Science Department, Brookhaven National Laboratory, Upton, New York 11973 USA

(Received 22 July 2008; revised manuscript received 8 February 2009; published 12 March 2009; corrected 13 March 2009)

Dynamic atomic force microscopy in the noncontact regime is used to study the morphology of a nonvolatile liquid (squalane) as it spreads along wettable nanostripes embedded in a nonwettable surface. Results show that the liquid profile depends on the amount of lateral confinement imposed by the nanostripes, and it is truncated at the microscopic contact line in good qualitative agreement with classical mesoscale hydrodynamics. However, the width of the contact line is found to be significantly larger than expected theoretically. This behavior may originate from small chemical inhomogeneity of the patterned stripes as well as from thermal fluctuations of the contact line.

DOI: 10.1103/PhysRevLett.102.106103 PACS numbers: 68.08.Bc, 68.15.+e, 68.37.Ps

The macroscopic spreading of a liquid droplet on a solid surface proceeds via the formation of a very thin ''precursor film'' ahead of the droplet's contact line [1]. Whether the liquid flow in this thin film can be described adequately by classical hydrodynamics is still a matter of debate. Indeed, a continuum description may not hold for films only a few molecules thick. Moreover, microscopic effects such as van der Waals fluid-solid attraction and thermal fluctuations are important in small dimensional liquid systems. By incorporating the effect of van der Waals attraction into classical hydrodynamic theory, de Gennes and coworkers have predicted [2] that the length of the precursor, L_P, for a simple liquid is approximately given by

$$L_P = a\sqrt{\frac{S}{\gamma}}\mathrm{Ca}^{-1}, \tag{1}$$

where $S = \gamma_{SV} - \gamma_{SL} - \gamma$ is the spreading parameter, which depends on the liquid surface tension γ and the solid-vapor and solid-liquid interfacial energies, respectively, γ_{SV} and γ_{SL}. $\mathrm{Ca} = \frac{\eta V}{\gamma}$ is the capillary number which depends on the liquid viscosity η and the spreading velocity V of the liquid. $a = \sqrt{2A/\gamma}$ is a molecular length scale depending on the Hamaker constant A. Moreover, the film thickness, h, is expected to decrease as the inverse of the distance from the apparent droplet contact line until the film is ''truncated'' at a thickness $h_0 = a\sqrt{\frac{3\gamma}{2S}}$ significantly larger than a molecular size since typically $S/\gamma \ll 1$. The truncation region corresponds to the *microscopic* contact line.

So far, experiments have only partially supported the above predictions without providing a conclusive picture. Early ellipsometry measurements found the precursor film thickness to agree only qualitatively with the inverse fall-off behavior [3] or to fall off too rapidly [4]. Much of the experimental results refer to the latest stages of the spreading process when the precursor film reduces to a monomolecular, diffuse film [5]. By using phase-modulated interference microscopy, Kavephour *et al.* [6] have measured L_P for viscous fluids over the range $10^{-6} < \mathrm{Ca} < 10^{-3}$ and found excellent agreement with Eq. (1) although the vertical and lateral resolution of the experiment were not sufficient to verify the inverse fall-off dependence of h. Unfortunately, the optical techniques used so far lack the lateral resolution necessary to unveil the morphology of the microscopic contact line. This limitation has also prevented the study of liquid spreading under nanometer-scale lateral confinement (i.e., in a quasi-one-dimensional geometry), another situation where the applicability of classical hydrodynamic theory is questionable. Addressing these questions is important for emerging technologies aiming at the formation and manipulation of smaller and smaller amounts of liquid [7].

Here atomic force microscopy (AFM) is used to record, with unprecedented spatial resolution, the morphology of nonvolatile liquid squalane ($C_{30}H_{62}$) spreading along wettable nanostripes embedded in a nonwettable surface. These results show that the liquid's height profile depends on the amount of lateral confinement imposed by the nanostripes, and it is truncated at the microscopic contact line, in good quantitative agreement with de Gennes' model.

The nanofluidic experiments described in this work were conducted on a model ''open nanofluidic device'' consisting of a series of interconnected wettable stripes embedded in the nonwettable (CH_3 terminated) surface of a octadecyltrichlorosilane (OTS) monolayer self-assembled on a silicon wafer [8]. This chemical pattern, sketched in Fig. 1(a), essentially consists of a reservoir pad R (sized 1×1 mm) connected to long ($5\ \mathrm{mm} \times 350\ \mu\mathrm{m}$) stripe $S1$. This stripe is constricted to a narrower stripe $S2$ (sized $100 \times 30\ \mu\mathrm{m}$) and eventually to a series of parallel nanostripes NS of width ranging from 100 to 600 nm and a length of approximatively 40 μm [see Fig. 1(b)]. The nanostripes open up into a wider stripe $S3$ (of size similar to $S2$) connected to the stripe $S4$ (of width similar to $S1$). The reservoir R and the stripes $S1$ and $S4$ were patterned by long (40 min.) exposure to short wavelength (184.9 and

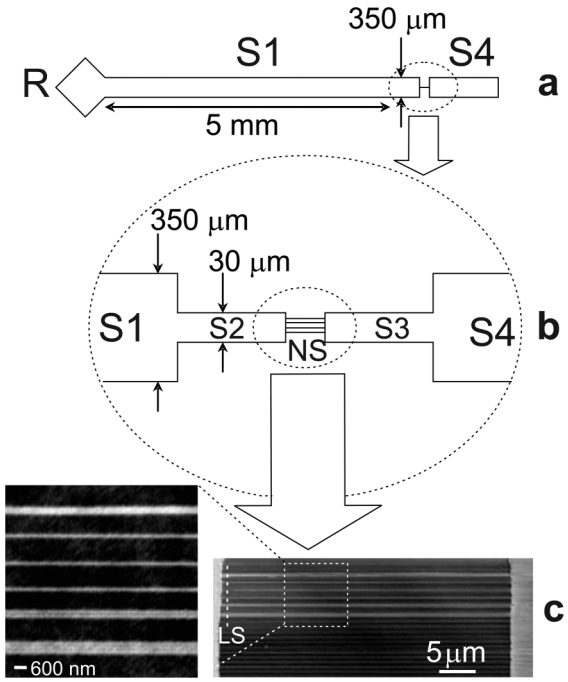

FIG. 1. (a) "Open nanofluidic device" consisting of a wettable reservoir pad R connected to a narrow (5 mm $\times$ 350 μm) wettable stripe both embedded in the nonwettable surface of an OTS monolayer. (b) The stripe $S1$ is constricted at its end to a narrower, wettable stripe $S2$ (size 100 $\times$ 30 μm) connected to a series of parallel nanostripes, NS, of width ranging from 100 to 600 nm. (c) A "friction force" AFM image shows the wettable nanostripes which appear as bright lines over the dark, methyl-terminated background.

253.7 nm) UV radiation through a lithographic mask in the presence of atmospheric oxygen [9].

The stripes $S2$, $S3$, and the nanostripes NS were patterned using AFM oxidative nanolithography [8,10]. Here, a metallic, biased, AFM tip contained in a humid environment is used to electrochemically oxidize the monolayer terminal methyl group to a carboxylic acid group. Stripes of varying widths were patterned by changing the bias (from 7 to 10 V) and the relative humidity (from 80% to 100%). Both UV and AFM lithography cause a moderate etching of the organic monolayer (respectively, $\approx$0.7 nm and $\approx$ 0.3 nm [10,11] as measured by AFM) comparable to the roughness of the native substrate. For this reason, the patterned stripes are more clearly imaged using friction force AFM imaging [10,11] as shown in Fig. 1(c). Friction force images were obtained by recording the twist of the AFM cantilever when the tip moves in contact with the sample surface. The nanoliquid morphology was imaged using amplitude-modulation [12] AFM in the noncontact regime [11,13]. To operate in this regime, which only involves long-range, attractive tip-sample interactions, the cantilever is modulated with a small amplitude (1–10 nm) at a fixed frequency about 100 Hz above the fundamental resonance (300 kHz).

The experiment is initiated when a small drop of liquid squalane is deposited on the reservoir pad and the liquid starts spreading along the stripe $S1$. The dynamics of the macroscopic spreading along $S1$ is studied using optical microscopy and a representative image which displays the advancing contact line is shown in Fig. 2. Analysis of multiple images provides the time-dependent velocity of the apparent contact line, $V \propto t^{-(0.55\pm0.5)}$. This is consistent with the results of Darhuber *et al.* [14]. Whereas the scaling exponent is independent on the amount of liquid deposited in the reservoir pad, the velocity increases with the reservoir volume. This allows one to vary the velocity V_0 of the contact line at the instant when the liquid reaches the end of $S1$ and the precursor film enters the nanostripes.

The presence of the precursor film at the entrance of the nanostripes was detected by repeatedly scanning the AFM tip across a single line which is transverse to the wettable nanostripes [dashed line LS in Fig. 1(c)]. Scanning only a line (rather than the entire surface occupied by the nanostripes) considerably improves the temporal resolution of the measurements up to about 0.5 s [15]. The line-scans (256 pixels) were collected at a frequency of 1.5 Hz and stacked together to form an "image" as shown in Fig. 3(a). In this picture, the vertical axis represents the transverse cross section of the stripes (with height shown in false-color scale) whereas the horizontal axis represents a time lapsing from left to right. Initially, the height contrast of the nanostripes is slightly negative and independent on the stripe width which indicates the absence of liquid on the stripes. Subsequently, the height contrast on the stripes becomes positive increasing continuously which is the evidence of the liquid spreading exclusively along the nanostripes. For the widest stripes, the rise in thickness occurs at slightly different times for different longitudinal profiles. This result suggests that the contact line may be somewhat rough in the transverse direction. This roughness may originate from nanoscale chemical inhomogene-

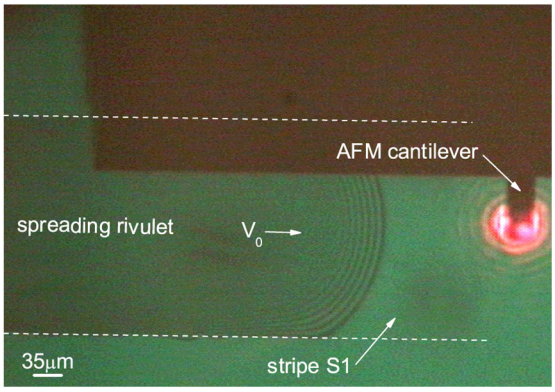

FIG. 2 (color online). Optical image showing the position of the apparent contact line spreading along the stripe $S1$ (whose boundaries are denoted by the dashed lines) as well as the location of the AFM tip.

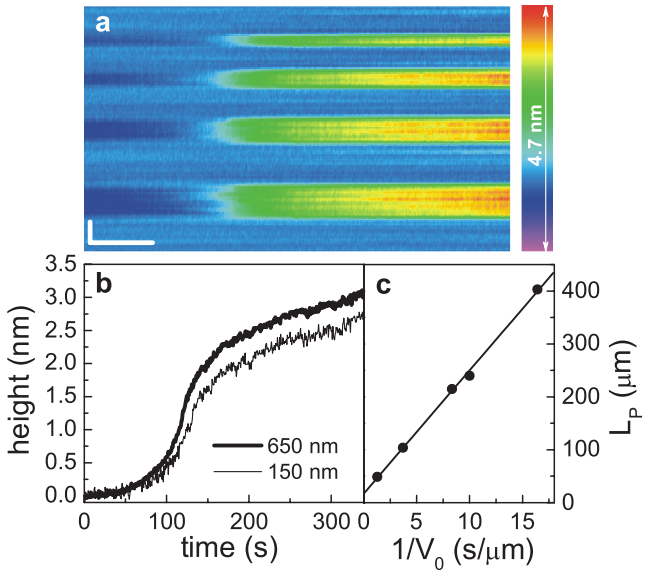

FIG. 3 (color online). (a) Temporal evolution of a transverse cross-sectional AFM profile of the nanostripes (lateral scale bar is 50 s, vertical scale bar is 400 nm). (b) Height of the liquid versus time on the thinnest (150 nm-wide, thin line) and thickest (650 nm-wide, thick line) stripe as extracted from (a). (c) The length of the precursor film, L_P, versus the inverse of the spreading velocity V_0. The line denotes a linear fit to the data.

ity of the patterned regions which leads to small, local variations of the film thickness.

The maximum liquid thickness on the thinnest (150 nm-wide) and thickest (650 nm-wide) stripe, as extracted from (a), are plotted as a function of time in Fig. 3(b) (thin and thick line, respectively). This represents a thickness which was obtained by averaging several profiles (4 for the thinnest and 15 for the thickest stripe) at different transverse positions. The plot shows that the temporal variation of film thickness is qualitatively the same on the wide and on the narrow stripes and that in both cases, the ''tip'' of the nanorivulet is not molecularly sharp. Initially, the liquid thickness grows slowly up to a value $\sigma \approx 0.7$ nm, about twice the lateral size of a squalane molecule [16]. Beyond this thickness, the data show an inflection point, and the growth becomes approximatively linear at longer times. In this regime, the maximum liquid thickness is found to depend on the stripe width; more specifically, the film is thinner (approximatively 0.4 nm) on the thinnest line. This is the effect of the nanoscale lateral confinement on the liquid morphology. The pinning of the contact line along the boundaries of the wettable stripe imposes a curvature to the liquid's free surface. The resulting capillary pressure must be compensated by the effective pressure (also known as disjoining pressure) due to van der Waals solid-liquid interactions [17]. Consequently, for sufficiently thin stripes, the film height is expected to decrease with the stripe width [11,17].

The extension L_P of the precursor film at the instant when the liquid reaches the nanostripes has been estimated from simultaneous optical and AFM measurements. An optical image (such as in Fig. 2) is taken at the instant when the film enters the stripes as observed with AFM [as shown in Fig. 3(a)]. L_P is obtained from this image by measuring the distance between apparent contact line and the position of the AFM tip on the plane of the substrate with an accuracy of a few micrometers. From these measurements, carried out at various velocities V_0, it is found that L_P scales as $1/V_0$ as shown in Fig. 3(c). This result is in excellent agreement with de Gennes' model, Eq. (1). Using a realistic value of $A = 1 \times 10^{-21}$ J [18] implies $a = 0.26$ nm. From the slope of the data in Fig. 3(c) (straight line) and using literature values of $\gamma = 0.029$ N/m and $\eta = 0.032$ Pa s (at 25 °C), one can estimate the spreading parameter $S = 3 \times 10^{-4}$ N/m.

The temporal evolution of the maximum liquid thickness on the nanostripes has also been recorded as a function of V_0, and representative results are illustrated in Fig. 4(a) for the 650 nm-wide stripe. The rate of growth of the liquid increases with V_0 as expected since the adiabatic precursor film is predicted to advance with the same velocity as the macroscopic contact line. From the optical measurements of V_0, it is known that this quantity is approximatively constant on the time scale of the AFM measurements (a few minutes). Moreover, Fig. 3(a) shows that the liquid's velocity inside the nanostripes, V_0^{ns}, is not significantly affected by confinement since the liquid is detected almost

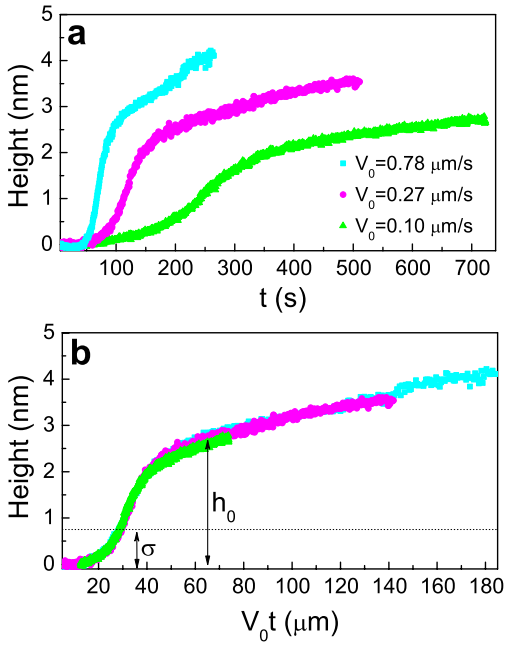

FIG. 4 (color online). (a) Growth rate of the maximum liquid thickness (color symbols) on a 650 nm-wide stripe for V_0 equal to 0.78 μm/s (cyan squares), 0.27 μm/s (magenta dots) and 0.10 μm/s (green triangles). (b) Height data as in (a) plotted versus the spatial coordinate $V_0 t$.

simultaneously inside all the nanostripes. Therefore, the ansatz is made that the velocity in the nanostripe regions is the same as in the region $S2$, $V_0^{\mathrm{ns}} \simeq V_0$. Thus, the liquid's height profile, shown in Fig. 4(b), is obtained by rescaling the abscissa in Fig. 4(a) by V_0.

In this region, all of the profiles exhibit nearly the same morphology, independent of the spreading velocity. This further supports the assumption $V_0^{\mathrm{ns}} \simeq V_0$. It also suggests that the profiles do not evolve significantly over time since very similar profiles were obtained for a range of velocities corresponding to collection times ranging from $\sim$30 minutes to $\sim$4 hours after deposition of liquid in the reservoir pad. The profile decreases very slowly with the distance from the macroscopic contact line until it is ''truncated'' at a thickness $h_0 = 2.7$ nm. Below h_0, the profile decreases rapidly until an inflexion point occurs at $h \approx \sigma$. The profile appears smooth, without terraces of thickness comparable to the molecular size, consistently with earlier ellipsometric studies [5]. This result suggests that the squalane chains do not orient in well-defined layers parallel to the substrate, possibly because the substrate roughness and the branched molecular structure of the liquid disrupt layering [18].

The liquid thickness at the truncation region, h_0, is in good quantitative agreement with de Gennes' model of precursor film in case of a finite S. Indeed, by using the equation $h_0 = a\sqrt{\frac{3\gamma}{2S}}$ and the experimental value of h_0, one obtains $S = 4 \times 10^{-4}$ N/m, consistent with the value obtained from the data in Fig. 3(c). However, the width of the microscopic contact line, defined as the distance over which the liquid thickness decreases from h_0 to σ, is about 10 μm, 3 orders of magnitude larger than predicted by the theory, $\Delta w = h_0^2/2a \approx 10$ nm [2]. This discrepancy could originate, at least partially, from the contact line roughness which reflects a slight chemical inhomogeneity of the substrate. However, the observed roughening gives rise to a rather small (about 5%) dispersion of the measured width around the average. Thermal fluctuations of the contact line may also be responsible for the line broadening. Indeed, recent theoretical works [19,20] have shown that these fluctuations give rise to an effective stochastic force that may increase the spreading rate as predicted by classical, deterministic hydrodynamics. Further experimental and theoretical work is required to clarify the origin of the contact line broadening.

This work presents time-resolved AFM measurements of the morphology of a liquid spreading under nanoscale confinement. Results show that the liquid profile is affected quantitatively by lateral confinement within 100 nm-wide wettable stripes whereas, independently on the amount of the confinement, the profile is truncated at the microscopic contact line in good quantitative agreement with mesoscale, continuum hydrodynamics. However, the width of the microscopic contact line exceeds considerably the value expected theoretically. These results improve our understanding of liquid flow on the nanoscale but also call for further theoretical modeling.

This work is supported by the Nanoscale Science, Engineering and Technology Program of the U.S. DOE under Contract No. DE-AC02-98CH10886. The author thanks B. Ocko, S. Dietrich, M. Rauscher, and J. Koplik for stimulating discussions.

*checco@bnl.gov

[1] W. Hardy, Philos. Mag. **38**, 49 (1919).
[2] P. G. de Gennes, Rev. Mod. Phys. **57**, 827 (1985).
[3] L. Leger, M. Erman, A. M. Guinet-Picard, D. Ausserre, and C. Strazielle, Phys. Rev. Lett. **60**, 2390 (1988).
[4] D. Beaglehole, J. Phys. Chem. **93**, 893 (1989).
[5] F. Heslot, A. M. Cazabat, and P. Levinson, Phys. Rev. Lett. **62**, 1286 (1989).
[6] H. P. Kavehpour, B. Ovryn, and G. H. McKinley, Phys. Rev. Lett. **91**, 196104 (2003).
[7] J. C. T. Eijkel and A. van den Berg, Microfluid. Nanofluid. **1**, 249 (2005).
[8] R. Maoz, S. Cohen, and J. Sagiv, Adv. Mater. **11**, 55 (1999), and references therein.
[9] S. W. Roberson, A. J. Fahey, A. Sehgal, and A. Karim, Appl. Surf. Sci. **200**, 150 (2002).
[10] A. Checco, Y. Cai, O. Gang, and B. M. Ocko, Ultramicroscopy **106**, 703 (2006).
[11] A. Checco, O. Gang, and B. M. Ocko, Phys. Rev. Lett. **96**, 056104 (2006).
[12] R. Garcia and R. Perez, Surf. Sci. Rep. **47**, 197 (2002).
[13] A. Checco, P. Guenoun, and J. Daillant, Phys. Rev. Lett. **91**, 186101 (2003).
[14] A. A. Darhuber, S. Troian, and W. W. Reisner, Phys. Rev. E **64**, 031603 (2001).
[15] A. Checco and B. Ocko, Phys. Rev. E **77**, 061601 (2008).
[16] J. Gao, W. D. Luedtke, and U. Landman, J. Chem. Phys. **106**, 4309 (1997).
[17] C. Bauer and S. Dietrich, Phys. Rev. E **60**, 6919 (1999).
[18] J. N. Israelachvili, *Intermolecular and Surface Forces* (Academic Press, New York, 1992).
[19] B. Davidovitch, E. Moro, and H. A. Stone, Phys. Rev. Lett. **95**, 244505 (2005).
[20] K. Mecke and M. B. Rauscher, J. Phys. Condens. Matter **17**, S3515 (2005).